PCCP
Physical Chemistry Chemical Physics

# Accepted Manuscript

This article can be cited before page numbers have been issued, to do this please use: M. Ord, Z. Lu, B. Allison and B. Liu, *Phys. Chem. Chem. Phys.*, 2026, DOI: 10.1039/D6CP00967K.




ROYAL SOCIETY OF CHEMISTRY

rsc.li/pccp

View Article Online
DOI: 10.1039/D6CP00967K

PCCP

ARTICLE TYPE

Cite this: DOI: 00.0000/xxxxxxxxxx

# Quantum Simulations of the Ballistic Motion of a Surface Adsorbate

Matthew Ord,[a] Ziyou Lu,[a] William Allison,[a] and Boyao Liu[a]*

Received Date
Accepted Date

DOI: 00.0000/xxxxxxxxxx

In thermal equilibrium, a surface adsorbate moves ballistically for short timescales and diffusively over longer timescales. The distinction between these regimes depends on the rate of energy transfer between the adsorbate and substrate, which is conventionally described in terms of friction. Motion in the ballistic regime is determined by the local adiabatic potential, independent of the friction, and measurements of ballistic motion should therefore reveal information about those local interactions. Here, we present a method for simulating ballistic motion by calculating the intermediate scattering function (ISF), which is directly accessible through experiment. We show, using a simple tight-binding argument, that the motion can be treated as that of an adsorbate with an effective mass, distinct from its actual mass. Furthermore, the effective mass is expected to be energy, and hence temperature, dependent. A more detailed quantum simulation demonstrates that the experimental ISF also depends on the initial state before scattering, a result that suggests it should be possible to identify the degree of localisation within the adsorbate site. These results establish a direct link between the quantum nature of the system and experiment, opening the door to future measurements.

## 1 Introduction

As a result of thermal stimulation, an adsorbate moves within and between adsorption sites according to the strength of its interactions in relation to the degree of thermal excitation. The motion is often treated as being entirely classical,[1–4] and most experimental studies have focused on diffusive behaviour, which occurs in the long-time limit.[5–8] In that regime, and especially at low temperatures with light adsorbates, quantum effects lead to an enhancement of the motion since they allow non-classical behaviour, such as tunnelling, as an additive factor to the classical rate of hopping over energy barriers.[9–12] Quantum effects in the motion over short times, the ballistic regime, have been noted recently in the case of atom transport through nano-tubes[13], and the significance of processes that do not lead to barrier crossings have been emphasised in classical systems[14,15], but we know of no other systematic work applied to the motion of adsorbates in the quantum regime.

As experimental techniques improve[16,17], measurements of ballistic motion will become possible. The present work is, therefore, devoted to an investigation of the phenomenology of quantum effects in the ballistic regime. We limit discussion to the thermally activated motion of an isolated adsorbate. The aim is to elucidate the likely behaviour and to illustrate how quantum effects, such as the band-structure for atomic motion and the quantum coherence of the adsorbate wavefunction, will be observable through experiment.

As an adsorbate particle moves on the surface, it is constantly interacting with the surrounding environment. Typically, the interactions between the particle and the environment are decomposed into a static equilibrium potential and a time-dependent frictional force. The dynamics can then be treated classically, for example using the Langevin and Fokker-Planck equation[18], or more accurately as an open quantum system.[19,20]

The random frictional force plays a crucial role in both classical and quantum models, as it leads to an exchange of energy between the system and environment. The state of the system is randomized over the timescale of the interaction, until it reaches a thermal equilibrium. In the quantum model, the frictional force also leads to decoherence, and therefore directly influences the equilibrium coherence length of the system. The origin of the friction force lies in interactions of the adsorbate with phonons and/or electrons in the substrate. Although they have different physical origins, frictional forces have previously been treated additively[18,21,22] so, in the present work, we treat them generically.

Here, our aim is to provide a connection to Helium Spin-Echo (HeSE) experiments[23] through simulations of the Intermediate Scattering Function (ISF)[24,25], which is the primary tool of analysis in experiment. To set the context for the analysis of ballistic motion, we begin with the simple classical system of a free particle in 1D. The ISF of such a classical system is defined as

$$I(\Delta k, t) = \langle e^{-i\Delta k x(0)} e^{i\Delta k x(t)} \rangle, \quad (1)$$

[a] Cavendish Laboratory, University of Cambridge, J J Thomson Avenue, Cambridge CB3 0US, United Kingdom. E-mail: bl476@cam.ac.uk

View Article Online
DOI: 10.1039/D6CP00967K



where $x(t)$ is the particle's position as a function of time, and $\langle ... \rangle$ represents an ensemble average. $I(\Delta k,t)$ provides us with information about the average behaviour of the particle on a length-scale determined by the value of $\Delta k$.

The dynamics may be modelled classically using a Langevin equation[4]

$$m\frac{\mathrm{d}}{\mathrm{d}t}x(t) = p(t) \quad \frac{\mathrm{d}}{\mathrm{d}t}p(t) = -\gamma p(t) - \nabla V(x(t)) + F(t). \tag{2}$$

The adsorbate interacts with the environment through a static potential $V(x(t))$ and through friction, which is characterized by a coefficient $\gamma$. The friction coefficient governs both the strength of dissipation, $\gamma p(t)$, and the stochastic force $F(t)$ which is described by a Markovian process

$$\langle F(t)F(t')\rangle = 2\gamma k_B T\,\delta(t-t'). \tag{3}$$

On a flat surface, $V(x) = 0$, and the ISF is given by[26]

$$I(\Delta k,t) = \exp\left(\Delta k^2 \frac{k_B T}{m\gamma^2}(1-\gamma|t| - e^{-\gamma|t|})\right). \tag{4}$$

Figure 1 shows the typical form of the ISF, along with its approximate form at long and short timescales. These are, respectively

$$I(\Delta k,t) = \exp\left(\Delta k^2 \frac{k_B T}{m\gamma^2}\right)\exp\left(-\Delta k^2 \frac{k_B T}{m\gamma}|t|\right) \quad \gamma|t| \gg 1, \tag{5}$$

and

$$I(\Delta k,t) = \exp\left(-\frac{k_B T}{2m}(\Delta k t)^2\right) \quad \gamma|t| \ll 1. \tag{6}$$

At long times, $\gamma|t| \gg 1$, the exponential decay is characteristic of a random walk, which we denote as the diffusive regime. While, at short times, $\gamma|t| \ll 1$, the ISF is Gaussian and completely independent of the frictional force. Equation (6) exactly matches the behaviour of a free classical particle in a closed system.[27] The short timescale, $\gamma|t| \ll 1$ is our definition of the ballistic regime, in which the dynamics of the adsorbate depend only on the initial values of $x$ and $p$ and the shape of the static background potential. The ISF then involves an ensemble average of the initial phase-space coordinates.

The distinction between the two timescales is crucial in our analysis. For long times the friction must be included explicitly and the adsorbate treated as an open quantum system[12,28]; however, for the short times of interest here, the adsorbate can be regarded as a much simpler, closed quantum system. Even in our closed quantum system, there is still a role for the friction as we show below. Frictional interactions affect the quantum coherence of the initial adsorbate state, which is something we explore further in section 6.

In the present manuscript, we will investigate the influence of quantum effects on the behaviour of the ballistic ISF, for which we need to develop a complete quantum mechanical description of the system. In the quantum regime, the ISF of a free particle is given by[21]

$$I(\Delta k,t) = \langle e^{-i\Delta k\hat{x}(0)} e^{i\Delta k\hat{x}(t)}\rangle, \tag{7}$$

where $\hat{x}(t)$, the position operator in the Heisenberg picture, replaces the usual classical position coordinate. To compare to experiment, the quantum mechanical expectation $\langle \ldots \rangle$ is taken over an ensemble average initial state represented by the density matrix $\hat{\rho}_{\text{average}}$. For an operator $\hat{O}$ the quantum mechanical expectation is

$$\langle \hat{O}\rangle = \sum_i \langle i|\hat{\rho}_{\text{average}}\hat{O}|i\rangle \tag{8}$$

for a set of basis states of the adsorbate $|i\rangle$.

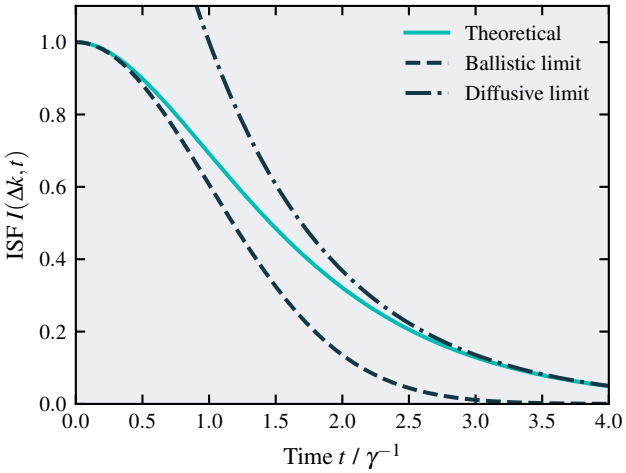


Fig. 1 The ISF $I(\Delta k,t)$ for a classical particle in thermal equilibrium in a flat landscape $V(x) = 0$, given by eq. (4). The solid line shows the complete ISF at a particular value of $\Delta k$, together with approximations for the diffusive limit, at long-times (dash-dot line), and the ballistic limit, at short-times (dashed line). In the ballistic regime the ISF has a Gaussian profile shown in eq. (6) and there is a clear separation between the ballistic and the diffusive regime.

Previous semi-classical simulations found that for Markovian friction the short timescale behaviour was independent of the strength of the frictional force.[21] We therefore consider the motion to be ballistic, which means the behaviour depends only on the initial state and the static interaction with the environment. Recently, a similar theoretical approach, using a closed quantum description of adsorbate motion, has been used to derive an ISF, $I(\Delta k,t)$, as a correlation function of thermal wave packets.[25] We adopt the same procedure to define the ISF but tackle the quantum dynamics differently.

Below, we develop a complete simulation of quantum ballistic motion. We will then use the simulation to investigate the influence that both the static background potential and the initial state of the system have on the ISF at short timescales. It is important to note that although the quantum dynamics in the ballistic regime is independent of friction, the initial state of the system depends on previous frictional interactions, which will determine the coherence length of the wavefunction, and hence the degree of localisation exhibited by the adsorbate. The simulations show a dependence on the initial state of the adsorbate and suggest that experiments should therefore be uniquely sensitive to that localisation.

## 2 Direct Simulations of a Ballistic ISF

Here we set out details of the method we use to perform direct simulations of ballistic motion. Following the approach taken in

View Article Online
DOI: 10.1039/D6CP00967K



ref.[25], we can write the average density matrix as a sum over states

$$\hat{\rho}_{\text{average}} = \sum_{l,r} \rho_{lr} |l\rangle\langle r| \tag{9}$$

By substituting this expression into eq. (7), we view the ISF as a sum over contributions from a large number of individual system states

$$I(\Delta k,t) = \sum_{l,r} \rho_{lr} I_{rl}(\Delta k,t) \tag{10}$$

$$I_{rl}(\Delta k,t) = \langle r|e^{-i\Delta k\hat{x}}\hat{U}(0,t)e^{i\Delta k\hat{x}}\hat{U}(t,0)|l\rangle, \tag{11}$$

where individual states of the system evolve according to $|\psi(t)\rangle = \hat{U}(t,t')|\psi(t')\rangle$. In the context of adsorbate motion the ISF, $I_{rl}(\Delta k,t)$, can be found in the classical limit by considering the behaviour of a thermal ensemble of Gaussian wavepackets[29]. As first noted by Heller et al.[29], each wavepacket will remain Gaussian during propagation and scattering which leads to a natural semi-classical interpretation. The formula is however more general, and can be applied to any quantum system.[25]

As discussed in section 1, in the ballistic regime the behaviour of the system does not depend directly on friction. We can therefore use simple Hamiltonian dynamics. In this model, the time evolution operator $U(t,t')$ is given by

$$\hat{U}(t,t') = \exp\left(-\frac{i\hat{H}(t-t')}{\hbar}\right) \quad \hat{H} = \frac{\hat{p}^2}{2m} + V(\hat{x}), \tag{12}$$

where $V(\hat{x})$ is the static background potential felt by the system, which will have the periodicity of the underlying surface.

To simulate the full ISF, we sample a large number ($N$) of initial left ($l_s$) and right ($r_s$) states, chosen at random such that

$$\langle\hat{\rho}_{\text{average}}\rangle \simeq \frac{1}{N}\sum_{s=1}^{N} |l_s\rangle\langle r_s|. \tag{13}$$

For each pair of left/right states, we calculate a contribution to the ISF $I_{rl}(\Delta k,t)$ by directly propagating the states $|l_s\rangle$ and $e^{i\Delta k\hat{x}}|r_s\rangle$ according to eq. (11). After a large number of samples, the simulation average ISF converges to the true $I(\Delta k,t)$.

In previous work[25], propagation of the left $|l\rangle$ and scattered right $e^{i\Delta k\hat{x}}|r\rangle$ state was achieved using the multi-configuration time-dependent Hartree (MCTDH) method.[30] In the current work we make use of direct eigenvalue decomposition to propagate the individual states of the system. In the Supplementary Information we provide a brief discussion of the relative merits of the two methds and further detail on the present calcuation. While eigenvalue decomposition is often less efficient than MCTDH, in a periodic system we can make use of Bloch's theorem to drastically reduce the cost of generating eigenstates[13].

## 3 Ballistic Motion on a Flat surface

In order to demonstrate the viability of our approach, we apply the methods in the preceding section and the Supplementary Information to the problem of motion on a flat surface. That is, with $V(\hat{x}) = 0$. The result for a classical particle was discussed in the introduction and an analytic result is known for the quantum case,[31] where a canonical ensemble is used as the average state of the system.

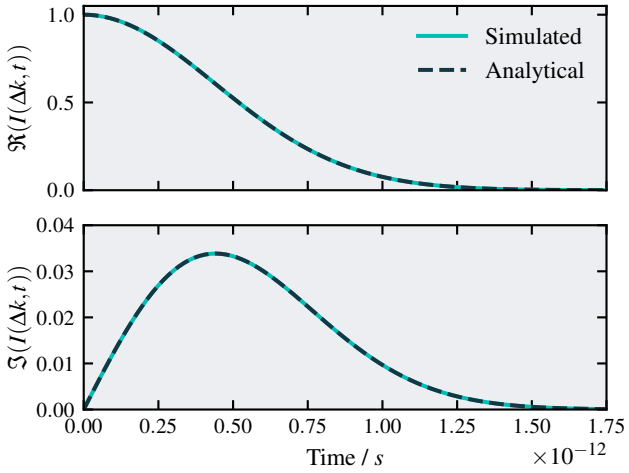


Fig. 2 The ballistic ISF for motion on a flat surface, $V(x) = 0$ calculated using the methods described in the main text (solid line). Both the real part (upper panel) and imaginary part (lower) are shown. The values we use correspond to scattering from a free Na atom in equilibrium at 155 K, and for a value of $\Delta k = 9.6 \times 10^9$ m$^{-1}$. The free particle ISF is known analytically[31] (shown as a dashed line) and is in excellent agreement with the simulations.

$$\hat{\rho}_{\text{average}} = \hat{\rho}_{\text{canonical}} = \frac{1}{Z}\sum_n \exp\left(-\frac{E_n}{k_BT}\right)|n\rangle\langle n|, \tag{14}$$

where $Z = \sum_n \exp(-E_n/k_BT)$. The ballistic ISF picks up a phase $\exp(-iE_rt/\hbar)$ in addition to the classical Gaussian decay

$$I(\Delta k,t) = \exp\left(-\frac{iE_rt}{\hbar}\right)\exp\left(-\frac{k_BT}{2m}(\Delta kt)^2\right) \quad E_r = \frac{\hbar^2\Delta k^2}{2m}, \tag{15}$$

an effect known as quantum recoil.[31]

To validate our approach, we start by simulating the behaviour of a free sodium atom. As suggested in ref.[25], we can calculate the ISF of such a system by selecting left and right states given by

$$|l\rangle = |r\rangle = |\psi(\vec{\theta})\rangle = \sum_{k_c,n} \exp\left(-\frac{E_n(k_c)}{2k_BT} + i\theta_{k_c,n}\right)|k_c,n(k_c)\rangle \tag{16}$$

where $0 \le \theta_{k_c,n} < 2\pi$ are a set of phases selected from a random uniform distribution, and $E_n(k_c)$ is the energy of $|k_c,n(k_c)\rangle$.

If we average over these phases $\theta$, we recover the required density matrix

$$\hat{\rho}_{\text{canonical}} = \langle|\psi(\vec{\theta})\rangle\langle\psi(\vec{\theta})|\rangle_{\vec{\theta}}. \tag{17}$$

The use of a thermal wavepacket is particularly well suited to our approach to simulating the ISF, as it provides an analytical formula for the eigenstate decomposition of initial and final states.

Figure 2 shows the real and imaginary parts of the simulated ISF, using 100 samples, in comparison to the analytic result.[31] It is clear that the simulation and analytic results are essentially identical, confirming the validity of our numerical approach.

View Article Online
DOI: 10.1039/D6CP00967K



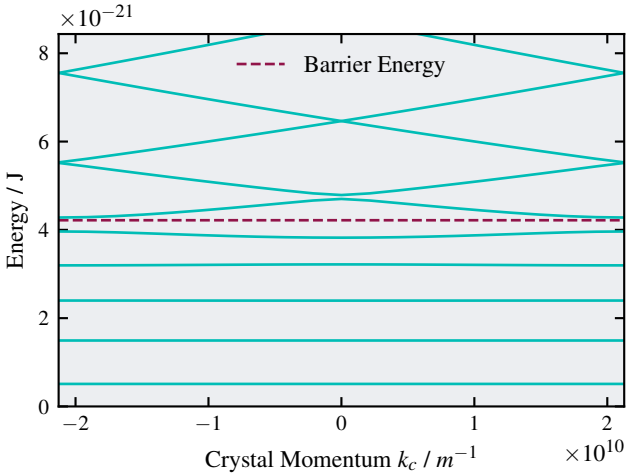


Fig. 3 Band structure of a 1D sinusoidal potential, with a barrier height of $4.22 \times 10^{-21}$ J. The barrier height, and size of the primitive unit cell, were chosen to match a Na adsorbate moving between three-fold sites on a Cu(111) surface with the barrier in the bridge position.[22]. Below the barrier energy (dashed horizontal line), the bands are significantly flattened, but they become more free-particle like at energies well above the barrier.

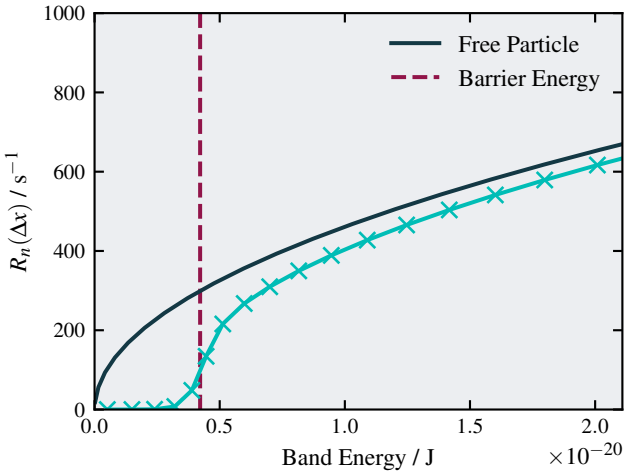


Fig. 4 The transition rate, $R_n(\Delta x)$, for band $n$ in the tight-binding model as a function of the average band energy. The 1D sinusoidal potential, shown in fig. 3, is used. The crosses and coloured solid line correspond to the sinusoidal band while the solid black line correspond to the expectations for a free particle. The transition rates for the two systems are converge at large band index, where the bands themselves are essentially the same as those of a free particle. However, the rates diverge progressively below the barrier energy of $4.22 \times 10^{-21}$ J, which occurs around a band index of 5-6.

## 4 A ballistic effective mass in a periodic potential

The introduction of a periodic potential modifies the band structure for adsorbate motion from that of a free particle to one where there are energy gaps, of varying degree, at the zone boundaries. Before moving to the detailed numerical calculation of the ISF, for which there is no analytic result, we explore the behaviour that might be expected through an analysis of ballistic motion in a single band. By doing so, we can define an effective mass, which is a function of the band index.

We begin with a generic, one-dimensional band structure and, use standard tight-binding arguments[32] together with a sinusoidal potential, since it captures the essence of the phenomenology and is used widely[12,13,15]. Figure 3 shows the band-structure of a 1D sinusoidal potential, with a classical barrier height of $4.22 \times 10^{-21}$ J, chosen to represent the case of Na adsorbed on a Cu(111) surface.[22,33]

Eigenstates from each band (indexed by $n$) are used to form a series of localised Wannier states, as typically used to understand the dynamics of electrons in solids[32,34]

$$|x_m, n\rangle = \sum_{k_c} \exp(i\phi_{k_c}) \exp(i x_m k_c) |k_c, n(k_c)\rangle \quad x_m = m\Delta x, \tag{18}$$

where the phases $\phi_{k_c}$ are chosen to minimize the spatial spread of the wavefunction.[34] Each state is localised on a single lattice site indexed by $m$, and we calculate the rate of transition between neighbouring states directly from the band structure, as follows. At small times, the state evolves according to

$$e^{i\hat{H}\Delta t/\hbar}|x_m, n\rangle \simeq (1 + i\frac{\Delta t}{\hbar}\hat{H})|x_m, n\rangle \tag{19}$$

and the probability, $P$, of moving from $x_0$ to $x_1$ in time $\Delta t$ is given by

$$\frac{\Delta x^2}{\Delta t^2} P(x_0 \to x_1, \Delta t) = \frac{\Delta x^2}{\hbar^2} |\langle x_1, n|\hat{H}|x_0, n\rangle|^2. \tag{20}$$

By substituting the wavefunction of the localized state (eq. (18)) into eq. (20) we find

$$\frac{\Delta x}{\hbar}\langle x_1, n|\hat{H}|x_0, n\rangle = \frac{\Delta x}{\hbar}\sum_{k_c} \exp(-i\Delta x k_c) E_n(k_c) = R_n(\Delta x), \tag{21}$$

which is how we define $R_n(\Delta x)$, the rate of transition from $x_0$ to $x_1$ in a single band of index $n$.

In order to generate an effective mass for motion in that band, we first consider the case of a free particle, $V(x) = 0$. The bands, in that case, can be written as

$$E_n(k_c) = \begin{cases} \frac{\hbar^2}{2m}\left(|k_c| + \frac{n\pi}{\Delta x}\right)^2 & n \text{ even}, \\ \frac{\hbar^2}{2m}\left(|k_c| - \frac{(n+1)\pi}{\Delta x}\right)^2 & n \text{ odd}, \end{cases} \tag{22}$$

and the transition rate for a particle in band $n$, follows from eq. (21) and is given by

$$R_n^{\text{free}}(\Delta x) = (-1)^{n+1}\frac{2\pi\hbar}{m\Delta x^2}\left(n + \frac{1}{2}\right), \tag{23}$$

where, $m$ is the mass of the free particle.

We now define an effective mass, $m_{eff}$, that characterizes the ballistic motion, for the case when $V(x) \neq 0$. We define the general transition rate as

$$R_n(\Delta x) = (-1)^{n+1}\frac{2\pi\hbar}{m_{\text{eff}}\Delta x^2}\left(n + \frac{1}{2}\right) \quad m_{\text{eff}} = \frac{R_n^{\text{free}}(\Delta x)}{R_n(\Delta x)}m, \tag{24}$$

where the effective mass, $m_{eff}$, follows from the ratio of the tran-

View Article Online
DOI: 10.1039/D6CP00967K



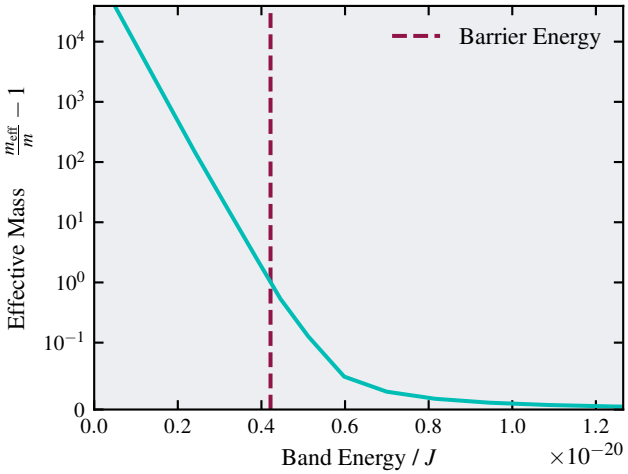


Fig. 5 Tight-binding effective mass, from eq. (24), plotted against the average energy of each band in the sinusoidal potential of fig. 3. Note that the effective mass, eq. (24), is plotted on a logarithmic scale as $m_{\rm eff}/m - 1$, and it grows exponentially below the barrier.

sition rates with and without the potential $V(x)$.

Figure 4 shows results for the transition rates, $R_n(\Delta x)$, of a sodium atom moving in different bands of the cosine potential shown earlier in fig. 3. Data points and the interpolated blue line correspond to motion in the cosine potential, while the solid line shows motion of a free particle having the same mass. For large values of the band index, $n \geq 10$, the behaviour in the cosine potential is essentially the same as that of a free particle, whereas for bands below the barrier height, $n \approx 4$, the transition rate decreases strongly. Figure 5 shows the same phenomenology in terms of the effective mass, $m_{\rm eff}$, from eq. (23), plotted against the average energy. Below the barrier energy (vertical bar), the calculated effective mass grows exponentially.

The motion within a single band is only part of the story, since a thermal average over all bands would be required to describe a system at a fixed temperature. With that proviso, we can conclude that the ballistic motion should provide information on the band-structure of the adsorbate motion, and that the behaviour will be strongly dependent on the band-energy, and hence the temperature of the system.

## 5 Ballistic Motion in 1D and 2D corrugated potentials

In the previous section, we outlined the general effect of a corrugated potential on ballistic motion. The calculation, which was performed for a 1D sinusoidal corrugation, gave an indication of the contribution to ballistic motion made by individual bands. Here, we extend that analysis to a thermally activated system. The rate of thermally activated ballistic motion is necessarily a complex thermal average over the occupied states, and will therefore require a complete simulation of the system. We use the wavefunctions defined in eq. (16) together with eq. (10) and eq. (11) to calculate the complete ISF.

Figure 6 shows the ISF for the potential used earlier ($E_b = 4.22 \times 10^{-21}$ J) for a canonical ensemble at a temperature of 155 K. That temperature corresponds to $k_B T \approx 2 \times 10^{-21}$ J, roughly half of the energy barrier. Thus, we expect the motion to be confined to a single adsorption site with infrequent transitions between sites, the so-called hopping regime. It is unsurprising that the ISF shown in fig. 6 is quite different from that of the free particle at the same temperature, shown previously in fig. 2. Specifically, the ISF, shown by solid lines in fig. 6, does not decay to zero in the time range illustrated, and there is an indication of oscillatory behaviour that is clearly evident in the real and imaginary parts of the ISF. An oscillatory ISF is a characteristic of inelastic scattering with a definite energy change, which one can attribute to inter-band transitions within the localised states below the barrier energy.

The initial decay is well approximated by a Gaussian function, whose width we take to represent the ballistic motion. To account for other, longer-term processes, we simply add a constant. The functional form we use is

$$I(\Delta k, t) = A(\Delta k) + B(\Delta k) \exp\left(-\frac{1}{2}\left(\frac{t}{C(\Delta k)}\right)^2\right), \qquad (25)$$

where the rate is taken to be $C(\Delta k)^{-1}$. A typical fit to the calculated ISF is shown as a dashed line in fig. 6, and the rates we obtain, as a function of $\Delta k$, are shown in fig. 7a for the 1D cosine potential.

Figure 7b shows the results for a hexagonal 2D potential[16,33] with the same barrier energy. While there are differences of detail between the 1D case and the 2D case, the overall trends in both panels of fig. 7 are similar, suggesting that the dimensionality of the diffusion does not affect the main conclusions of our work. A significant feature of fig. 7 is that the ballistic rate for the free particle ($E_b = 0$) lies below that of the system with a sinusoidal energy barrier ($E_b > 0$). In Section 4, it was shown that bands below the barrier have a low group velocity; consequently they appear as a constant background to the ISF, and are incorporated within the $A(\Delta k)$ term in eq. (25). In contrast, bands lying above $E_b$ have group velocities well above the thermal average resulting in a faster decay than the free-particle average.

The inference from fig. 7, that the initial rate for the corrugated system lies above that of the free system, is robust to changes in the shape of the underlying potential and to changes in the mass of the adsorbate. We conclude that, in general, the ISF of the corrugated system is more complex and difficult to interpret than that of a simple free system. In performing these calculations we assumed a particular form for the initial thermal wavefunctions, as specified in eq. (16). In the next section we explore the consequences of such a choice.

## 6 Localisation and Coherence in Thermal Wavefunctions

The wavefunctions used earlier, eq. (16) are not the only ensemble average states capable of representing physical reality. In thermal equilibrium, we require the eigenstates to be occupied according to the Boltzmann distribution

$$P_n = \langle n|\hat{\rho}_{\rm average}|n\rangle = \frac{1}{Z}\exp\left(-\frac{E_n}{k_B T}\right). \qquad (26)$$

View Article Online
DOI: 10.1039/D6CP00967K



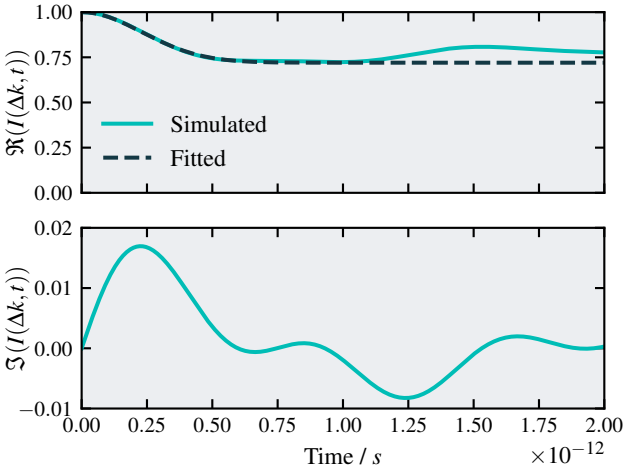


Fig. 6 A plot of the simulated ballistic ISF for a temperature of 155 K and $\Delta k = 9.6 \times 10^9$ m$^{-1}$ for a Na atom in the sinusoidal potential of fig. 3. The real part and imaginary part are shown as solid lines in the upper and lower panel respectively. In comparison with a free Na atom, fig. 2, the ISF decreases much less, as low energy states are effectively confined by the potential. However, the initial drop is well approximated by a Gaussian function, shown by the dashed line.

The condition is, however, satisfied by any density matrix of the form

$$\hat{\rho} = \hat{\rho}_{\text{canonical}} + \hat{M}, \tag{27}$$

where

$$\langle n|\hat{M}|n\rangle = 0, \quad \forall n. \tag{28}$$

Here, the matrix $\hat{M}$ can be related to the amount of coherence between eigenstates of the system. We expect a real system to exhibit some degree of spatial coherence, as localised states are typically more robust to decoherence by the environment.[35] In contrast, the canonical ensemble provides a coherent superposition of delocalised states, which may not accurately represent the state of a real system. The effect of coherence, specifically localisation, induced by interactions of the adsorbate with its environment is something that has not previously been studied in detail. Our aim is to demonstrate that the degree of adsorbate localisation directly influences the form of the ISF in the ballistic regime, and hence on the experimental observations.

To explore the influence of coherence on the shape of the ISF, we slightly modify the approach taken in section 5. Starting with the thermal wavepacket

$$|l\rangle = |r\rangle = |\psi(\vec{\theta})\rangle = \sum_{k_c,n} \exp\left(-\frac{E_n(k_c)}{2k_BT} + i\theta_{k_c,n}\right)|k_c, n(k_c)\rangle, \tag{29}$$

we can select angles $\theta_{k_c,n}$ from a biased distribution, such that for $(k_c,n) \neq (k_c',n')$

$$\hat{M}_{(k_c,n),(k_c',n')} = \exp\left(-\frac{E_n(k_c)+E_{n'}(k_c')}{2k_BT}\right)\langle e^{i(\theta_{k_c',n'}-\theta_{k_c,n})}\rangle. \tag{30}$$

To generate a set of localised initial states, we use the projection approach suggested in ref.[34]. We start by generating a trial wavefunction $|\psi(x_0,k_0)\rangle$, a Gaussian function localised at a particular classical coordinate $(x_0,k_0)$

$$\langle x|\psi(x_0,k_0)\rangle = \exp\left(-\left(\frac{x-x_0}{\sigma}\right)^2\right)\exp(ik_0x). \tag{31}$$

By calculating a set of phases $\theta_{k_c,n} = \arg(\langle k_c,n|\psi(x_0,k_0)\rangle)$ we generate a Boltzmann state that is localised around $x_0$.

Figure 8a illustrates the effect of our procedure. In the main panel, the target Gaussian function is shown as a dashed line, localised in $x$ near $1.3 \times 10^{-10}$ m. The corresponding thermalised wavefunction, $\langle x|\psi\rangle$ is shown as a solid line. The wavevector, $k$, dependence of the target and thermalised wavefunctions is shown in the inset.

To show the effects of coherence and localisation on the ballistic ISF, we use a series of initial states, like the one in fig. 8a, that are preferentially localised around the lattice site. The calculation was performed for a value of $\Delta k = 3.2 \times 10^{10}$ m$^{-1}$.

Figure 8b shows the ISF calculated with localised initial states (solid line) compared to that obtained with the non-localised canonical ensemble (dashed line). We observe a significant change in the ballistic behaviour between the two sets of initial states. It follows that the nature and extent of the change in the ISF depends on the degree of localisation and the distribution of localisation centres.

When the calculation is repeated for the case of a free adsorbate, $E_b = 0$, we find no change in the ballistic behaviour when localised and non-localised states are used. While that finding may have been predictable, the result demonstrates the importance of localisation in corrugated systems of the type commonly encountered in experiment. It suggests that localisation is only relevant when the length-scale is comparable to the lattice constant of the surface. A complete simulation of diffusion, using for example the stochastic wavefunction approach outlined in ref.[28] would be required to predict the initial states of a real system accurately.

## 7 Discussion and Conclusions

In the present manuscript we have used a closed-quantum system to predict the ballistic motion of an adsorbate. Our justification is that, by analogy with a classical system obeying a Langevin equation, the motion is independent of the friction on a sufficiently short time scale, i.e. when $\gamma|t| \ll 1$, where $\gamma$ is the friction. Thus, at short times, thermal interactions can be neglected and the open quantum system that represents the adsorbate motion can be replaced with a closed system. The procedure allows us to investigate the effects of the spatially periodic interactions due to the surface lattice and the resulting systems are sufficiently simple for us to compare a 1D corrugated energy landscape with the behaviour that might be observed in a 2D system. Our results, for example those shown in fig. 7, indicate that the dimensionality changes the detail to be observed rather than the general trends that occur.

Consideration of the band-structure in which the adsorbate moves on our periodic surface indicates that individual states within the bands will contribute to the ballistic motion depending on the local band curvature. Specifically, states below the barrier

View Article Online
DOI: 10.1039/D6CP00967K



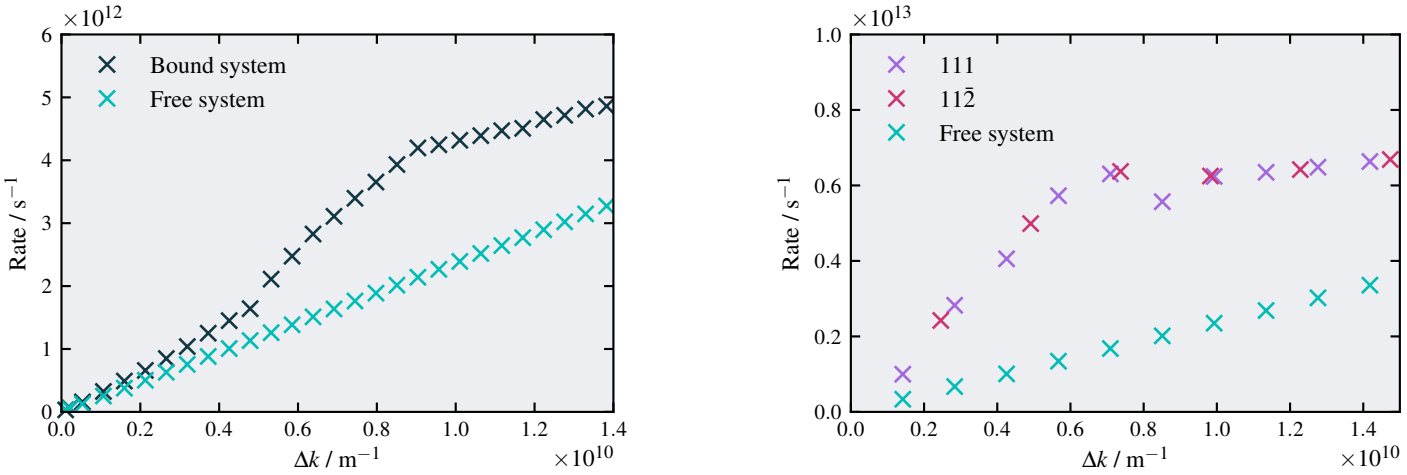


(a) 1D System (b) 2D System

Fig. 7 Simulated decay rates for ballistic motion in 1D (a), and 2D (b). In both cases the systems are designed to approximate the motion of a Na atom on a Cu(111) surface. Thus the barrier to inter-cell motion is identical in both cases. The 1D band-structure is shown in Figure 3 and the 2D potential is created with a single parameter (energy barrier) and hexagonal symmetry.[16] Rates for the corresponding free systems are shown (blue data points) for comparison. In both the 1D and 2D cases the ISF initially decays at a faster rate than the free system, which we ascribe to an over-sampling of the contribution from the higher momentum free particle eigenstates with energy above the barrier.

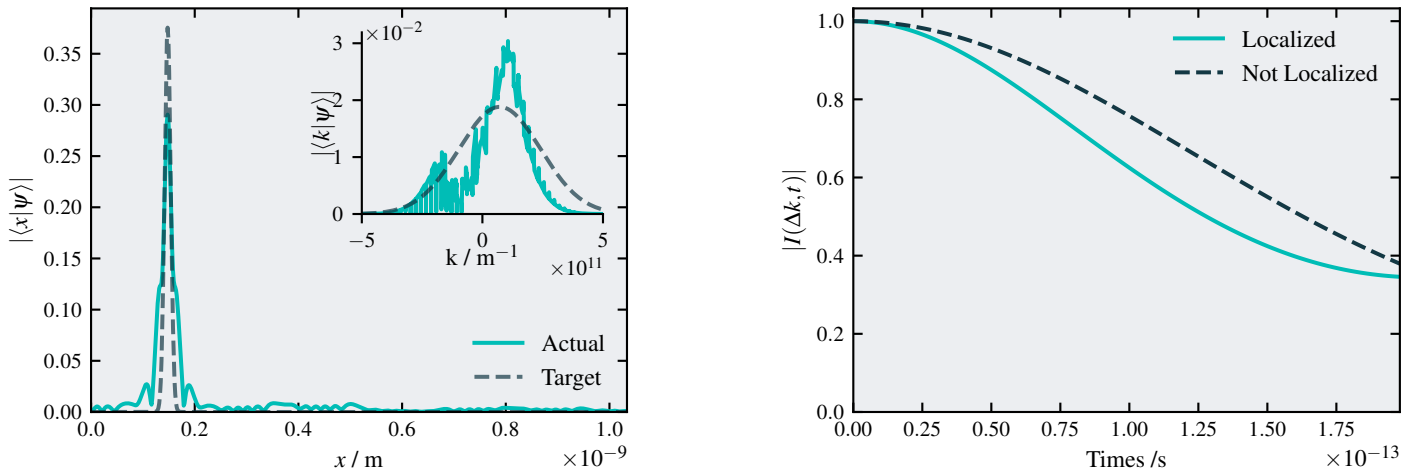


(a) localised State (b) Modified ISF

Fig. 8 The effect of localisation of the initial states. (a) illustrates the process used to generate a thermalised and localised initial state. The localised state (solid curve) is created by projecting onto a trial Gaussian wavefunction (dashed line). (b) shows examples of the ISF at $\Delta k = 3.2 \times 10^{10}$ m$^{-1}$ with $E_b = 4.22 \times 10^{-21}$ J. The solid blue line corresponds to localised initial states, while the dashed line is for non-localised initial states. The significant difference between these two cases illustrates that experiment should be sensitive to the finite coherence length of the system.

View Article Online
DOI: 10.1039/D6CP00967K



to inter-cell motion, being localised, have smaller curvature and therefore a lower group-velocity than those well above the barrier, which are effectively like a free particle. A simple analysis, using a sinusoidal potential with a barrier, $E_b$, of inter-cell motion, combined with a tight-binding approach was performed to calculate transition rates. The result suggests that the ballistic rate varies dramatically with the band index and gives an effective mass that increases exponentially for the states that lie below the energy barrier (see fig. 5). Since the occupancy of the bands is temperature dependent, it seems likely that the net ballistic motion will, therefore, be strongly affected by the system temperature.

Calculating the full ISF reveals a more complex picture. The calculations (see, for example, fig. 6) show a clear Gaussian dependence at very small times followed by complex, oscillatory features that appear to correspond to inter- and intra-band transitions giving rise to inelastic scattering. The initial Gaussian decay suggests a ballistic rate faster than that of the corresponding free particle, which we attribute to preferential sampling of higher-energy states.

That behaviour led us to consider the effect of coherence and localisation in the choice of wavefunction used in the calculation. We have constructed wavefunctions that are thermally equilibrated at a given temperature, yet localised within an adsorption site, that is around the minimum energy of the sinusoidal potential. When used to determine an ISF, the behaviour of these wavefunctions is significantly different from a simple non-localised thermal state (see fig. 8). The result suggests that in an experiment the observed ballistic behaviour will be sensitive to the initial state, according to some ensemble average, and hence the degree of localisation of the adsorbate. That, in turn, will depend on the coherence of the thermal wavefunction, which arises from the effect of friction in the open quantum system.[36] The coherence length is a property that is directly influenced by the stochastic interactions with the environment, and therefore a full diffusive simulation may be required to accurately predict coherence in a real system.

These results demonstrate that the short-time ballistic regime is rich with information regarding the quantum nature of the adsorbate. By understanding how the static potential and the initial coherence length shape the ISF, the present work provides a crucial theoretical foundation for interpreting future high-resolution scattering experiments.

## Author contributions

Matthew Ord: Conceptualization, Methodology, Project administration, Software, Writing - original draft. Ziyou Lu: Software. William Allison: Supervision, Writing - review & editing. Boyao Liu: Project administration, Validation, Writing - review & editing.

## Conflicts of interest

There are no conflicts to declare.

## Data availability

The code used in this study can be found at `https://doi.org/10.5281/zenodo.19051774`.

## Acknowledgements

We thank Salvador Miret-Artés and Elena Torres-Miyares for helpful discussions about stochastic effects in adsorbate diffusion. We are also extremely grateful to David J. Ward, John Ellis and Andrew P. Jardine for their contributions to our thinking on the topic and particularly for the connection of the present work to the corresponding experiments involving Helium Spin Echo (HeSE). M.O. is grateful for financial support from the Sims Fund, and to Fitzwilliam College, Cambridge for a Research Scholarship. B.L. is grateful to Gonville and Caius College, Cambridge for the provision of a Junior Research Fellowship. The work was performed in part at CORDE, the Collaborative R&D Environment established to provide access to physics related facilities at the Cavendish Laboratory, University of Cambridge.

## References

1 O. M. Braun and R. Ferrando, *Phys. Rev. E*, 2002, **65**, 061107.
2 R. Ferrando, M. Mazroui, R. Spadacini and G. E. Tommei, *New Journal of Physics*, 2005, **7**, 19.
3 M. Diamant, S. Rahav, R. Ferrando and G. Alexandrowicz, *Journal of Physics: Condensed Matter*, 2015, **27**, 125008.
4 N. Avidor, P. Townsend, D. Ward, A. Jardine, J. Ellis and W. Allison, *Computer Physics Communications*, 2019, **242**, 145–152.
5 G. Antczak and G. Ehrlich, *Surface Diffusion*, Cambridge University Press, 2010.
6 R. Ferrando and A. P. Jardine, in *Surface Diffusion*, ed. M. Rocca, T. Rahman and L. Vattuone, Springer, 2020, pp. 45–70.
7 J. Kelsall, P. S. M. Townsend, J. Ellis, A. P. Jardine and N. Avidor, *Phys. Rev. Lett.*, 2021, **126**, 155901.
8 P. Seiler, A. J. R. Payne, N. F. Xavier Jr, L. Slocombe, M. Sacchi and A. Tamtögl, *Nature Communications*, 2025, **16**, 10465.
9 P. Ohresser, H. Bulou, S. S. Dhesi, C. Boeglin, B. Lazarovits, E. Gaudry, I. Chado, J. Faerber and F. Scheurer, *Phys. Rev. Lett.*, 2005, **95**, 195901.
10 A. P. Jardine, E. Y. M. Lee, D. J. Ward, G. Alexandrowicz, H. Hedgeland, W. Allison, J. Ellis and E. Pollak, *Physical Review Letters*, 2010, **105**, 136101.
11 E. M. Mcintosh, K. T. Wikfeldt, J. Ellis, A. Michaelides and W. Allison, *J. Phys. Chem. Lett*, 2022, **12**, 48.
12 W. Guan, Y. Liu and Q. Shi, *Journal of Physical Chemistry C*, 2025, **129**, 1149–1156.
13 A. Ambrosetti, P. L. Silvestrelli, J. F. Dobson and L. Salasnich, *Physical Review B*, 2026, **113**, 035445.
14 A. Lyons, A. Devi, N. Q. Hoffer and M. T. Woodside, *Physical Review X*, 2024, **14**, 011017.
15 A. J. Archer, T. Ala-Nissila, T. J. Honour and S. P. Fitzgerald, *Journal of Chemical Physics*, 2025, **163**, 064105.
16 D. Ward, *PhD thesis*, University of Cambridge, 2013.
17 J. Zhu, *PhD thesis*, University of Cambridge, 2015.
18 T. Ala-Nissila, R. Ferrando and S. C. Ying, *Advances in Physics*, 2002, **51**, 949–1078.
19 S. C. Badescu, S. C. Ying and T. Ala-Nissila, *Physical Review*

View Article Online
DOI: 10.1039/D6CP00967K

*Letters*, 2001, **86**, 5092–5095.

20 E. E. Torres-Miyares, G. Rojas-Lorenzo, J. Rubayo-Soneira and S. Miret-Artés, *Phys. Chem. Chem. Phys.*, 2022, **24**, 15871–15890.

21 R. Martínez-Casado, A. S. Sanz and S. Miret-Artés, *The Journal of Chemical Physics*, 2008, **129**, 184704.

22 S. P. Rittmeyer, D. J. Ward, P. Gütlein, J. Ellis, W. Allison and K. Reuter, *Physical Review Letters*, 2016, **117**, 196001.

23 A. P. Jardine, H. Hedgeland, G. Alexandrowicz, W. Allison and J. Ellis, *Progress in Surface Science*, 2009, **84**, 323–379.

24 A. Rahman, *Phys. Rev.*, 1963, **130**, 1334–1336.

25 O. Bindech, F. Gatti, S. Mandal, R. Marquardt and J. C. Tremblay, *Molecular Physics*, 2025, e2541793.

26 S. Miret-Artés and E. Pollak, *Journal of Physics: Condensed Matter*, 2005, **17**, S4133.

27 J. Ellis, A. P. Graham and J. P. Toennies, *Phys. Rev. Lett.*, 1999, **82**, 5072–5075.

28 E. E. Torres-Miyares, D. J. Ward, G. Rojas-Lorenzo, J. Rubayo-Soneira, W. Allison and S. Miret-Artés, *Physical Chemistry Chemical Physics*, 2023, **25**, 6225–6231.

29 E. J. Heller, J. R. Reimers and G. Drolshagen, *Physical Review A*, 1987, **36**, 2613–2627.

30 M. H. Beck, A. Jäckle, G. A. Worth and H. D. Meyer, *Physics Reports*, 2000, **324**, 1–105.

31 R. Martínez-Casado, A. S. Sanz and S. Miret-Artés, *The Journal of Chemical Physics*, 2008, **129**, 184704.

32 N. W. Ashcroft and N. D. Mermin, *Solid state physics*, Philadelphia, PA : Saunders College : CBS Publishing Asia Ltd., 1976.

33 L. Padilla-Campos, A. Toro-Labbé and J. Maruani, *Surface Science*, 1997, **385**, 24–36.

34 N. Marzari, A. A. Mostofi, J. R. Yates, I. Souza and D. Vanderbilt, *Reviews of Modern Physics*, 2012, **84**, 1419–1475.

35 W. H. Zurek, *Physics today*, 1991, **44**, 36–44.

36 W. H. Zurek, *Reviews of Modern Physics*, 2003, **75**, 715–775.



View Article Online
DOI: 10.1039/D6CP00967K

The code used in this study can be found at https://doi.org/10.5281/zenodo.19051774.